Spectral Properties of Correlated Materials: Local Vertex and Nonlocal Two-Particle Correlations from Combined *GW* and Dynamical Mean Field Theory

Thomas Ayral,[1,2,3] Philipp Werner,[4,1] and Silke Biermann[2,5]
[1]*Theoretical Physics, ETH Zurich, 8093 Zürich, Switzerland*
[2]*Centre de Physique Théorique, Ecole Polytechnique, CNRS UMR7644, 91128 Palaiseau Cedex, France*
[3]*Institut de Physique Théorique (IPhT), CEA, CNRS, URA 2306, 91191 Gif-sur-Yvette, France*
[4]*Department of Physics, University of Fribourg, 1700 Fribourg, Switzerland*
[5]*Japan Science and Technology Agency, CREST, Kawaguchi 332-0012, Japan*
(Received 21 May 2012; published 28 November 2012)

We present a fully self-consistent combined *GW* and dynamical mean field (DMFT) study of the extended two-dimensional Hubbard model. The inclusion of the local dynamical vertex stemming from the DMFT self-energy and polarization is shown to cure the known problems of self-consistent *GW*. We calculate momentum-resolved spectral functions, two-particle polarizations, and electron-loss spectra, as well as the effective dynamical interaction induced by nonlocal screening. The momentum-dependence introduced by *GW* into the extended DMFT description leads to a narrowing of the quasiparticle width and more pronounced Hubbard bands in the metallic regime as one approaches the charge-ordering transition. It further affects the shape of collective modes, giving rise to dispersive plasmon-like long-wavelength and stripe modes.

DOI: 10.1103/PhysRevLett.109.226401 PACS numbers: 71.27.+a, 72.15.Qm, 75.20.Hr

Modern spectroscopic techniques are able to measure one- and two-particle spectra of condensed matter systems with remarkable precision, characterizing not only quasiparticle excitations but unveiling also satellite structures. Examples include Hubbard bands in photoemission spectroscopy, stemming from the atomic-like behavior of the electrons in partially filled narrow d or f shells [1], or collective excitations such as plasmonic features. Addressing such effects requires an accurate description of one- and two-particle spectral functions within the framework of many-body theory. The quantitative prediction of satellite features has even been used as a quality marker for many-body techniques. The failure of self-consistent perturbation theory in the screened Coulomb interaction, the self-consistent *GW* approximation, to describe plasmon satellites in the electron gas, for example, has provided arguments in favor of a non-self-consistent (''one-shot *GW*'') treatment [2–4]. For real solids, few fully self-consistent calculations are available [5,6], and no consensus concerning the virtues of self-consistency has been reached so far. A popular scheme, dubbed quasiparticle self-consistent (QPSC) *GW* [7] yields reasonable estimates both for total energies and spectra. Yet, most of the calculations within this scheme were applied to semiconductors, and applications to correlated metals only start to appear [8]. The inclusion of an appropriate vertex correction is expected to resolve the ambiguities around the self-consistency question, and it has been in particular proposed that a combined *GW* and dynamical mean field scheme [9] would enable self-consistent calculations even for spectral properties. Early pioneering calculations on a three-dimensional extended Hubbard model [10,11] have benchmarked several flavors of combined schemes along these lines. However, the numerical difficulty of solving the DMFT equations with frequency-dependent interactions has until now prevented the direct investigation of spectral properties.

Implementing the GW + DMFT scheme in a fully self-consistent manner for the two-dimensional extended Hubbard model, we here demonstrate that this technique indeed successfully overcomes the deficiencies of *GW*. The implicit inclusion of a nonperturbative local vertex enables fully self-consistent calculations for spectral properties. In the correlated metal regime, the GW + DMFT self-energy encodes both band renormalization effects and Hubbard satellite features. The theory also describes the Mott insulating state for strong local Coulomb interaction, which is inaccessible in *GW* alone, as well as the charge-ordered state driven by intersite interactions, absent from standard DMFT. We calculate the effective local interaction, containing the dynamical screening from nonlocal processes, and demonstrate how these give rise to plasmonic features in the local spectral function. Close to the charge-ordering transition, the nonlocal self-energy contributions stemming from *GW* lead to a considerable enhancement of quasiparticle weights. We analyze momentum-resolved two-particle spectra and show that the self-consistent combination of *GW* and *extended* dynamical mean field theory (EDMFT) strongly affects the shape of collective modes, giving rise to dispersive plasmon-like long-wavelength modes and stripe modes.

We consider the half-filled extended Hubbard model on a two-dimensional square lattice,

$$H = -t \sum_{i \neq j,\sigma} c^{\dagger}_{i\sigma} c_{j\sigma} + \sum_i (U n_{i\uparrow} n_{i\downarrow} - \mu n_i) + \frac{V}{2} \sum_{i \neq j} n_i n_j,$$

where $c_{i\sigma}$ and $c^{\dagger}_{i\sigma}$ denote the annihilation and creation operators of a particle of spin $\sigma = \uparrow, \downarrow$ at the lattice site i, $n_{i\sigma} = c^{\dagger}_{i\sigma} c_{i\sigma}$, and $n_i = n_{i\uparrow} + n_{i\downarrow}$. $\sum_{i \neq j}$ is the sum over all nearest-neighbor sites, $t > 0$ is the hopping amplitude between two neighboring sites, μ is the chemical potential, U the on-site repulsion between electrons of opposite spin and V the repulsion between two electrons on neighboring sites. The Fourier-transformed bare interaction term thus reads $v_k = U + 2V[\cos(k_x) + \cos(k_y)]$. All energies are given in units of the half-bandwidth $D = 4t$. We show results for inverse temperature $\beta D = 100$, restricting our study to the paramagnetic phase.

The GW + DMFT approach is derivable from a free energy functional [12]. The Legendre transform of the free energy with respect to the Green's function G and the screened interaction W [13] can be expressed as a sum of the Hartree-Fock part and a Luttinger-Ward-like correlation functional $\Psi[G, W]$, which sums up all skeleton diagrams built from G and W [14]. The GW + DMFT scheme consists in approximating Ψ as $\Psi \approx \Psi^{\mathrm{EDMFT}}[G_{ii}, W_{ii}] + \Psi^{GW}_{\mathrm{nonloc}}[G_{ij}, W_{ij}]$, where the first term is calculated from a (dynamical) impurity problem as in EDMFT [15–17] and the second term is the nonlocal ($i \neq j$) part of the GW functional $\Psi^{GW}_{\mathrm{nonloc}}[G_{ij}, W_{ij}] = -\sum_{i,j} G_{ij} W_{ij} G_{ji} + \sum_i G_{ii} W_{ii} G_{ii}$.

The GW + DMFT scheme self-consistently constructs the Green's function G and the screened interaction W of the system as a stationary point of the free energy functional. The self-energy Σ and polarization P are formally obtained by functional differentiation of Ψ with respect to G and W, leading to the expressions $\Sigma(k, i\omega) = \Sigma_{\mathrm{imp}}(i\omega_n) + \Sigma^{GW}_{\mathrm{nonloc}}(k, i\omega)$ and $P(k, i\nu_n) = P_{\mathrm{imp}}(i\nu_n) + P^{GW}_{\mathrm{nonloc}}(k, i\nu_n)$ (ω_n and ν_n are fermionic and bosonic Matsubara frequencies, respectively). This endows GW + DMFT with conserving properties [18]. The momentum-dependent G and W are then calculated from the one- and two-particle Dyson equations and used as inputs for a GW calculation, yielding $\Sigma^{GW} = -G \cdot W$ and $P^{GW} = 2G \cdot G$ (the dot denotes a convolution in frequency-momentum space and the factor 2 comes from the spin degeneracy). Their local parts are extracted to compute the local Weiss fields $\mathcal{G}$ and $\mathcal{U}$: $\mathcal{G}^{-1}(i\omega_n) = G^{-1}_{\mathrm{loc}}(i\omega_n) + \Sigma_{\mathrm{imp}}(i\omega_n)$ and $\mathcal{U}^{-1}(i\nu_n) = W^{-1}_{\mathrm{loc}}(i\nu_n) + P_{\mathrm{imp}}(i\nu_n)$. These, in turn, are used as inputs to a *dynamical* impurity model, which we solve using a continuous-time Monte Carlo algorithm [19,20] to obtain updated local self-energies. The whole scheme, summarized in Fig. 1, is iterated until convergence. The calculations have been performed on a 64×64 momentum grid, while the analytical continuation of the imaginary-time data has been performed using the maximum entropy method [21] in the spirit of Ref. [22]. We monitor the following quantities:

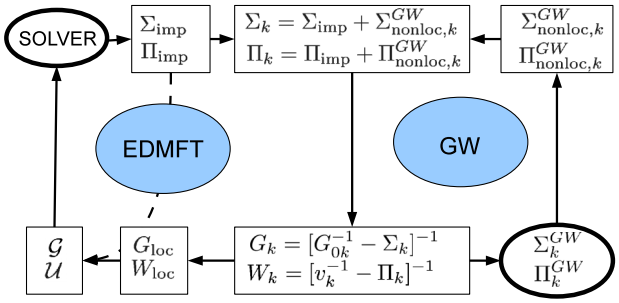

FIG. 1 (color online). Flow chart of the GW + DMFT scheme.

(i) the local spectral function $A_{\mathrm{loc}}(\omega) = -\frac{1}{\pi} \mathrm{Im} G_{\mathrm{loc}}(\omega)$, (ii) the momentum-resolved spectral function, (iii) the electron energy-loss spectrum (EELS) $\mathrm{Im}[-\epsilon(k, \omega)^{-1}]$ [where $\epsilon(k, \omega) = 1 - v_k P(k, \omega)$ is the dielectric function], and (iv) the effective dynamical interaction $\mathcal{U}$, which takes into account screening processes induced by V.

Within extended DMFT and GW + DMFT, in the absence of intersite repulsion, the Mott transition takes place at $U_c \approx 2.5$. This value is slightly modified by intersite repulsions $V < V_c = 0.8$. At V_c a transition to a charge-ordered phase occurs [23]. In the following we study the local spectral properties in the metallic phase with weak ($U = 0.5$, $V = 0.1$) and intermediate ($U = 2$, $V = 0.4$) interactions, as well as in the Mott insulator at $U = 3.5$ and $V = 3$. Figure 2 shows the local spectral function $A_{\mathrm{loc}}(\omega)$ obtained within (i) (self-consistent) EDMFT, (ii) self-consistent GW + DMFT (iii) self-consistent GW, and (iv) QPSC GW. The latter scheme was implemented by computing the lattice Green's function from the GW self-energy via $G(k, i\omega_n)^{-1} = i\omega_n - Z_k[\epsilon_k - \mathrm{Re}\Sigma_{GW}(k, i\omega_0)]$, where $Z_k \approx (1 - \mathrm{Im}\Sigma_{GW}(k, i\omega_0)/\omega_0)^{-1}$ is the quasiparticle weight as estimated from the value of the self-energy at the first

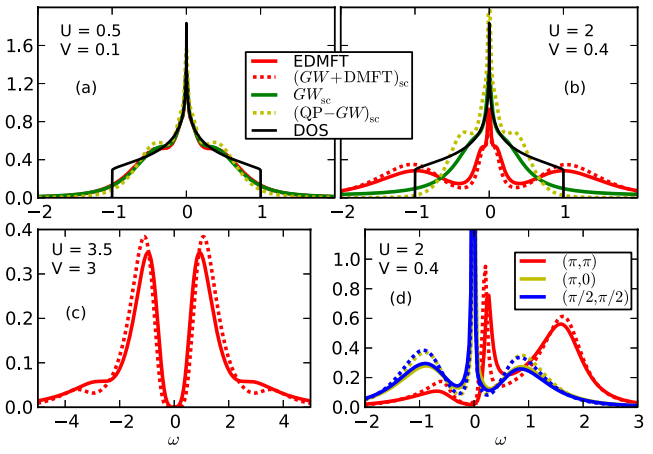

FIG. 2 (color online). Panels (a) to (c): spectral function $A_{\mathrm{loc}}(\omega)$ obtained within different self-consistent schemes (see text). Panel (d): spectral function at selected k points (solid line: EDMFT; dotted line: GW + DMFT).

Matsubara frequency. For small interactions [panel 2(a)], correlation effects are negligible, and the four schemes result in indistinguishable spectra within the numerical accuracy. As the local interaction U becomes significant [panel 2(b)], the width of the coherent central peak shrinks, and the corresponding spectral weight is transferred to higher energies. This (physically expected) behavior is realized by the EDMFT and GW + DMFT spectra, which exhibit higher-energy structures at $\omega \approx \pm U/2$. These Hubbard bands gain spectral weight as U increases further. The (integrated) quasiparticle weight Z goes from 0.44 (0.32) at $U = 1.5$, $V = 0.4$ for EDMFT (GW + DMFT) to 0.21 (0.12) at $U = 2$, $V = 0.4$. At $U = 3.5$, a Mott gap has opened, and the EDMFT and GW + DMFT spectra are similar [panel 2(c)]. In addition to the two Hubbard bands, the EDMFT and GW + DMFT spectra display two symmetric high-energy satellites, whose spectral weight depends on the intersite interaction V. The QPSC GW spectra display only a weak renormalization of the bandwidth as U increases from the weak to the strong coupling limit, and at all correlation levels the spectra remain metallic. The same is true within the self-consistent GW method (where the quasiparticle weight goes from 0.74 at $U = 1.5$, $V = 0.4$ to 0.67 at $U = 2$, $V = 0.4$). Here, with increasing correlations, some spectral weight is shifted to higher frequencies, albeit in a featureless way.

These observations show that both self-consistent GW approaches yield a correct result only in the weak-correlation regime. As correlations increase, GW fails to describe the shift of spectral weight to high-energy incoherent bands, present in DMFT. We note that in the local GW + DMFT spectra the Hubbard bands are enhanced compared to the EDMFT or GW spectra. This effect can be ascribed to the self-consistency, which allows the local quantities to readjust to the nonlocal self-energies Σ_{GW} and P_{GW}.

EDMFT and GW + DMFT spectra exhibit high-energy satellites in the Mott phase, which reflect the frequency dependence of the local interaction $\mathcal{U}(\omega)$ induced by the nearest-neighbor repulsion term V. The real part of this interaction is shown for the metallic phase in panel (c) of Figure 3. A sharp pole in $\mathcal{U}(\omega)$ (such as a plasmon pole) leads to multiple satellites in the local spectral function [22]. In our case, the $\mathcal{U}(\omega)$ are characterized by a broad continuum of poles centered at some energy ω_d, resulting in only two symmetric satellites in the Mott spectra [see Fig. 2(c)]. In the metallic phase, these satellites are present, but they are broad and merged with the Hubbard bands, making them hardly distinguishable.

The failure of both self-consistent GW schemes to capture Hubbard bands or high-energy satellites is consistent with the well-known observation that self-consistency in GW for the homogeneous electron gas results in a smearing out and displacement of high energy satellite features [3]. In light of this observation, most modern GW schemes

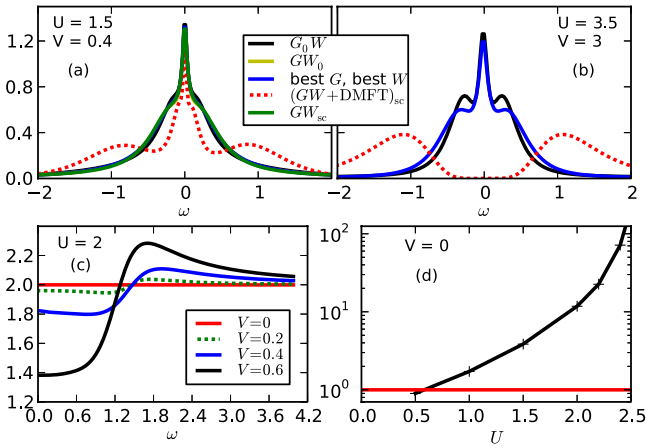

FIG. 3 (color online). Panels (a) and (b): Spectral function $A_{\mathrm{loc}}(\omega)$ obtained using 3 different one-shot GW schemes (see text). Panel (c): $\mathrm{Re}\mathcal{U}(\omega)$ obtained from EDMFT for different values of V. Panel (d): vertex estimate $\Lambda(\omega = 0)$ as a function of U.

therefore adopt a "best-G–best-W" strategy, rather than aiming at full self-consistency. Figure 3 illustrates the virtues and limitations of this strategy by displaying the spectra obtained in different one-shot GW schemes: (i) in "G_0W," the noninteracting Green's function G_0 and the converged GW + DMFT W are taken as inputs to a one-shot GW calculation, (ii) "GW_0" takes the converged GW + DMFT G and $W_0 = v(1 - vG_0G_0)^{-1}$ evaluated within the random-phase approximation as inputs and (iii) "best G, best W" takes the converged GW + DMFT G and W as inputs. At all correlation levels ($U = 1.5$ to $U = 3.5$), these three GW schemes produce results very similar to self-consistent GW. In particular, they remain metallic [at $U = 0.5$ (not shown), they are completely identical]. In the Mott phase ($U = 3.5$), even the "best G, best W" scheme yields a metallic self-energy, despite the Mott-like character of the input G and W. This phenomenon is due to the lack of Hedin's three-legged vertex Λ in GW schemes, as shown in Fig. 3(d). There, an estimate of the local part of Λ is computed from EDMFT results at $V = 0$. Remembering that, schematically, the irreducible vertex function Λ appears in the self-energy as $\Sigma = GW\Lambda$ [2], a rough estimate—neglecting the true frequency structure—is computed as follows: one computes an effectively vertex-corrected screened interaction $\tilde{W}(\tau) = \Sigma_{\mathrm{imp}}(\tau)/G_{\mathrm{imp}}(\tau)$ from EDMFT, then Fourier transforms it to $\tilde{W}(i\nu_n)$; finally, the static vertex estimate is obtained as $\Lambda(0) \approx \tilde{W}(i\nu_0)/W_{\mathrm{loc}}(i\nu_0)$. Crude as it is (the full vertex depends on two independent frequencies), this estimate nonetheless clearly demonstrates the role of vertex corrections for the Mott transition: from unity in the weakly correlated regime, it increases with U until it diverges at the Mott transition. This indicates that within the language of Hedin's equations, the divergence of the local vertex is the driving force of the Mott

phenomenon, making any vertexless approximation unfit to capture it.

The effect of the nonlocal GW contributions on EDMFT are illustrated by the momentum-resolved spectral functions, displayed in Fig. 2(d). In the presence of a strong intersite interaction, the nonlocal self-energy and polarization lead to a k-dependent modulation of the linewidth and weights. Compared to EDMFT, the GW + DMFT spectra display a strong sharpening of the quasiparticle peak along with an enhanced weight of the Hubbard bands. The impact of the GW diagrams becomes very strong on the brink of the charge-ordering transition.

We now turn to a study of two-particle quantities. Figure 4 shows the momentum-resolved imaginary part of the polarization and the electron energy-loss (EELS) spectrum $\mathrm{Im}[-\epsilon^{-1}(k,\omega)]$ in the metallic regime. Within EDMFT, the polarization displays a broad mode which reflects the particle-hole excitations of the system. They are centered at $U/2$, reflecting the emergence of the Hubbard bands and the corresponding excitations between Hubbard bands and the quasiparticle peak. In contrast, the polarization spectrum within GW + DMFT is dispersive. While displaying sharper features close to the $\Gamma \equiv (0,0)$ point, it captures particle-hole excitations due to Fermi-surface nesting at wave vector (π,π), as well as the zero-sound mode at long wavelengths and low energies. The EELS spectrum contains the particle-hole excitations (poles of the polarization) of the system and its collective modes, which correspond to the solutions of $\mathrm{Re}P(k,\omega) = 1/v_k$. These collective modes are damped out close to particle-hole excitations [when $\mathrm{Im}P(k,\omega)$ is large]. This analogue of the free-electron-gas Landau damping occurs at the (π,π) point in EDMFT and GW + DMFT. It can be directly ascribed to the nearest-neighbor repulsion, which induces scattering along this direction. The energy and lifetime of this collective excitation differs from EDMFT to GW + DMFT. In GW + DMFT it is lower in energy, more dispersive and with a larger lifetime. In GW + DMFT, two modes are visible above the $(\pi, 0)$ point, indicating the existence of two stripe modes at energies $\omega = 1$ and $\omega = 2$ corresponding to stripe-like modulations, where the sign of the density fluctuation varies from row to row in the x direction. For obvious reasons, they are not captured by EDMFT. These two-particle excitations are directly related to the screening in the system as the screened interaction, W, is given by $W(k,\omega) = \epsilon^{-1}(k,\omega)v_k$. In particular, they explain the retardation effects in the local interactions $\mathcal{U}(\omega)$ and the corresponding satellites in the local spectra.

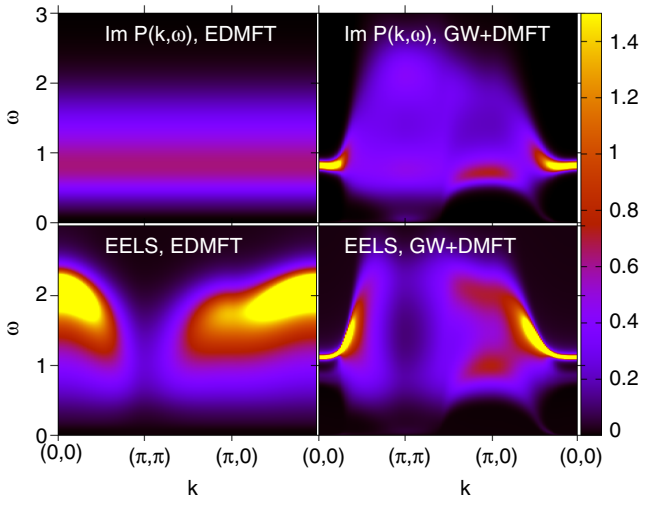

FIG. 4 (color online). $U = 2$, $V = 0.4$. Upper panels: $\mathrm{Im}P(k,\omega)$ within EDMFT (left) and GW + DMFT (right). Lower panels: $-\mathrm{Im}\epsilon^{-1}(k,\omega)$ within EDMFT (left) and GW + DMFT (right).

In conclusion, based on a fully self-consistent implementation of the combined GW + DMFT scheme, we have analyzed one- and two-particle satellite features in correlated materials. While we confirm the well-known "washing out" of satellite features in self-consistent GW calculations, self-consistent GW + DMFT does not suffer from this deficiency. Plasma- and zero-sound-like oscillations involving itinerant carriers as in the electron gas survive only in the regime of small local Coulomb interactions, but are quickly suppressed in the correlated metal. In this regime, excitations related to the creation of doublons become dominant. The momentum-dependence self-consistently introduced by the GW part becomes crucial when assessing dispersions of two-particle spectral properties, differentiating in particular the nature of the collective modes in the $(0,0)$, $(0,\pi)$, and (π,π) regions [24]. Our findings have implications for the nature of satellite features in correlated materials. In particular, it becomes obvious that electron-gas-like plasmons in materials stem dominantly from the charge contained in completely filled shells (that is from multiorbital effects), while partially filled shells give rise to doublon excitations of the kind we describe. Concerning the long-term goal of GW + DMFT calculations for realistic systems, the importance of this study is to demonstrate the ability to *calculate* the effective dynamical Coulomb interactions (rather than assuming a Hubbard U parameter) fully from first principles, in a self-consistent manner. Last but not least, the interplay of local correlations and charge-ordering phenomena and their intriguing wave-vector dependence that we evidence in this simple but generic model may already have been observed in two-dimensional materials: recent experimental findings of charge ordering in cuprates [25], cobaltates [26] or in systems of adatoms on surfaces [27] are prominent examples.

We acknowledge useful discussions with F. Aryasetiawan, M. Casula, A. Georges, P. Hansmann, M. Imada, M. Katsnelson, A. Millis, and T. Miyake. This work was supported by the French ANR under project SURMOTT, GENCI/IDRIS Orsay under Project

No. 1393, by DFG FOR 1346 and by the Swiss National Science Foundation (Grant No. PP0022-118866). Most of the calculations have been performed on the Brutus cluster at ETH Zurich, using a code based on ALPS [28]. We thank L. Boehnke for allowing us to use his MaxEnt code.

[1] M. Imada, A. Fujimori, and Y. Tokura, Rev. Mod. Phys. **70**, 1039 (1998).
[2] L. Hedin, Phys. Rev. **139**, A796 (1965).
[3] U. von Barth and B. Holm, Phys. Rev. B **54**, 8411 (1996).
[4] B. Holm and U. von Barth, Phys. Rev. B **57**, 2108 (1998).
[5] W. Ku and A. G. Eguiluz, Phys. Rev. Lett. **89**, 126401 (2002).
[6] A. Kutepov, K. Haule, S. Y. Savrasov, and G. Kotliar, Phys. Rev. B **82**, 045105 (2010).
[7] T. Kotani, M. van Schilfgaarde, and S. V. Faleev, Phys. Rev. B **76**, 165106 (2007).
[8] A. Kutepov, K. Haule, S. Y. Savrasov, and G. Kotliar, Phys. Rev. B **85**, 155129 (2012).
[9] S. Biermann, F. Aryasetiawan, and A. Georges, Phys. Rev. Lett. **90**, 086402 (2003).
[10] P. Sun and G. Kotliar, Phys. Rev. B **66**, 085120 (2002).
[11] P. Sun and G. Kotliar, Phys. Rev. Lett. **92**, 196402 (2004).
[12] S. Biermann, F. Aryasetiawan, and A. Georges, *Physics of Spin in Solids: Materials, Methods, and Applications*, NATO Science Series II (Kluwer Academic Publishers B. V, Dordrecht, Boston, London, 2004), pp. 43–65.
[13] This bosonic propagator, defined after a Hubbard-Stratonovich decoupling of the whole interaction term, is different from the one discussed in Ref. [10], which stems from the decoupling of the intersite interaction term only. The formulation in terms of W allows us to treat the on-site and the intersite interaction on the same footing.
[14] C. Almbladh, U. von Barth, and R. van Leeuwen, Int. J. Mod. Phys. B **13**, 535 (1999).
[15] A. M. Sengupta and A. Georges, Phys. Rev. B **52**, 10295 (1995).
[16] Q. Si and J. L. Smith, Phys. Rev. Lett. **77**, 3391 (1996).
[17] H. Kajueter, Ph.D. thesis, Rutgers University, New Brunswick, 1996.
[18] G. Baym, Phys. Rev. **127**, 1391 (1962).
[19] P. Werner and A. J. Millis, Phys. Rev. Lett. **99**, 146404 (2007).
[20] P. Werner and A. J. Millis, Phys. Rev. Lett. **104**, 146401 (2010).
[21] M. Jarrell and J. Gubernatis, Phys. Rep. **269**, 133 (1996).
[22] M. Casula, A. Rubtsov, and S. Biermann, Phys. Rev. B **85**, 035115 (2012).
[23] T. Ayral, S. Biermann, and P. Werner, arXiv:1210.2712.
[24] Interestingly, the self-consistency matters: we checked explicitly that a one-shot computation of the momentum-dependent polarization function based on a converged EDMFT Green's function G leads to a notably different result than the self-consistent one.
[25] T. Wu, H. Mayaffre, S. Kramer, M. Horvatic, W. N. Berthier, Claude and-Hardy, R. Liang, D. A. Bonn, and M.-H. Julien, Nature (London) **477**, 191 (2011).
[26] I. R. Mukhamedshin, H. Alloul, G. Collin, and N. Blanchard, Phys. Rev. Lett. **94**, 247602 (2005).
[27] P. Hansmann, L. Vaugier, and S. Biermann, J. Phys. Cond. Matt. (to be published).
[28] B. Bauer *et al.*, J. Stat. Mech. (2011), P05001.